Article

Steric paper based ratio-type electrochemical biosensor with hollow-channel for sensitive detection of Zn^{2+}

Li Li, Yan Zhang, Lina Zhang, Shenguang Ge, Mei Yan, Jinghua Yu

PII: S2095-9273(17)30349-3
DOI: http://dx.doi.org/10.1016/j.scib.2017.07.004
Reference: SCIB 175

To appear in: *Science Bulletin*

Received Date: 16 April 2017
Revised Date: 9 May 2017
Accepted Date: 19 June 2017

Please cite this article as: L. Li, Y. Zhang, L. Zhang, S. Ge, M. Yan, J. Yu, Steric paper based ratio-type electrochemical biosensor with hollow-channel for sensitive detection of Zn^{2+}, *Science Bulletin* (2017), doi: http://dx.doi.org/10.1016/j.scib.2017.07.004

Article

Received 16 April, 2017

Revised 9 May, 2017

Accepted 19 June, 2017

Steric paper based ratio-type electrochemical biosensor with hollow-channel for sensitive detection of Zn^{2+}

Li Li [a,1], Yan Zhang [a,1], Lina Zhang [b], Shenguang Ge [a,b], Mei Yan [a], Jinghua Yu[a,*]

[a]School of Chemistry and Chemical Engineering, University of Jinan, Jinan 250022, China

[b]Shandong Provincial Key Laboratory of Preparation and Measurement of Building Materials, University of Jinan, Jinan 250022, China

[*] Corresponding author. E-mail: ujn.yujh@gmail.com

[1] These authors contributed equally to this work.

ABSTRACT

The construction of flexible platform possessing the functions of immobilizing, separating, rinsing, and high-throughput analysis plays a significant role in biological and clinical research. Herein, hollow-channel technique was integrated with lab-on-paper for the simultaneous determination of two different concentrations of Zn^{2+} based on the origami principle, in which microfluidic channels were first patterned on a cellulose paper using commercial solid-state wax printer. Hollow-channels were created by laser cutting method as the role of both injecting ending and reaction tank. After screen printing three electrodes system, the resulting planar paper sheets were then folded into steric structures and functionalized by in-situ synthesized reduced graphene oxide. As a proof-of-concept, such lab-on-paper

device was employed in the ratiometric electrochemical monitoring of zinc ion from the environment and HepG2 cells extract, by combining with co-catalysis of porous metal-organic frameworks and hemin/G-quadruplex toward H_2O_2 in the linear range of 0.1−7,000 nmol/L. The results indicated that integrating hollow-channel with steric lab-on-paper offered a new methodological approach for the development of metal ions monitoring research. It is believed that it could be useful for various point-of-care related research fields, such as, on-site environmental monitoring, food safety, and disease diagnosis.

Keywords: Flexible platform, Lab-on-paper device, Ratiometric electrochemical monitoring, Zinc ion

1. Introduction

Paper-based microfluidic devices (PMDs), incorporating the simplicity, portability, and disposability of paper-strip tests with the multi-function and analysis of conventional lab-on-a-chip devices for analyte detection, have emerged as a promising solution to the need for low-cost diagnostic systems [1-7]. Some drawbacks, however, existing in traditional PMD are low rates of convective mass transfer and significant nonspecific adsorption due to the high surface area of the cellulose fibers. Hollow-channel based lab-on-chip devices, as newly arise platform which developed by Crooks's group [8] become popular in recent years. And now, they are widely applied for the determination of cancer biomarkers, glucose and bovine serum albumin (BSA) assays [9-11]. In this work, a high-throughput analysis pattern was first introduced into PMDs having hollow channels to analyze the target object, which laid a significant foundation for the development of various portable paper-based devices.

Recently, trace metal ions in the cells and the environment becomes one of the important concerns due to their assignable function in the biological system and deleterious effects on the public health [12-14]. Zinc ion, as an essential element required by all cells, plays a significant role in gene transcription and neural signal

transmission [15-17]. Therefore, developing methods for selective determination of zinc ions in living systems are of central importance. For this purpose, a variety of techniques, including neutron activation techniques [18], fluorescence methods, colorimetric methods have been developed for the determination of Zn^{2+} [19]. However, a universal problem lurked in colorimetric detection is that it can only be used in qualitative or semi-quantitative measurement and is unable to give accurate results [20,21]. Several other methods could hardly work without specific devices which were normally exorbitant, and intricate, and thus not applied to point-of-care (POC) testing. Thus, a new technology is in urgent need for user-friendly and precise detection of Zn^{2+}. An innovative way inspired by dual-wavelength fluorescent ratiometric method integrating ratiometric electrochemistry with steric PMDs was first proposed, which may be a preferred technique since no complicated equipment was required and the built-in correction of internal reference signal could eliminate the environmental interferences. To the best of our knowledge, there is no report on the establishment of high-throughput ratiometric PMDs for the zinc ion detection have been published.

As a class of promising hybrid functional materials, porous metal-organic frameworks (MOFs) have caused extensive concern since they were discovered [22-29]. They present many unique properties with unprecedentedly large and permanent inner porosity, and especially their pore size and surface functionality can be easily tuned upon selection of different metal ions and organic bridging ligands [30-34]. Accordingly, MOFs have been widely used in many fields, such as gas storage and separation, catalysis, drug delivery and sensing [35-38]. Currently, a series of porous iron-porphyrinic MOF ($(Fe\text{-}P)_n$-MOF) have been synthesized and used in analytical field for detection of H_2O_2 and ascorbic acid due to their super peroxidase activity [39]. In this work, to further enhance its catalytic performance, three-step amplification strategies were adopted. Firstly, reduced graphene oxide (rGO) with large surface area was in situ synthesized on the paper-based working electrode (rGO-PWE) through electro-reduction process, which could not only increase the conductivity of the device (Fig. S1 online) but also aggrandize amount of fixed

$(Fe\text{-}P)_n$-MOF, thus dramatically enhanced its catalytic properties. Secondly, rolling circle amplification (RCA) [40-43] as well as hemin were integrated for generating vast repeated hemin/G-quadruplex structure, which acted as HRP-mimicking DNAzyme. Thirdly, strong co-catalysis of MOF and hemin/G-quadruplex toward H_2O_2 were observed for the first time and integrated in one system as effective approach for advancing catalytic activity.

In this work, a flexible steric lab-on-paper device was demonstrated by incorporating origami skill as well as intelligently designing the configuration of fluid flow passage. Three-step amplification strategies and ratiometric electrochemistry made great contributions to the excellent sensitivity and a wide linear region for analysis of Zn^{2+}. Two paper working zones on a small piece of paper were applied to determine two different concentrations of Zn^{2+} simultaneously, which could not only simplify operation process and shorten experiment time, but also cost savings. We believe that this novel ratiometric paper based device will open a new horizon for the rational devise integrated platforms with the distinct features of maximum functionality at minimized size and weight, and broaden the potential applications of lab-on-chip device in POC testing.

2. Experimental

2.1. Materials and methods

Graphene oxide (GO), 5,10,15,20-tetrakis(4-carboxyl)-21 H,23H-porphyrin (TCPP), *N*,*N*-dimethylformamide (DMF), $FeCl_3 \cdot 6H_2O$, and chitosan ($\geqslant$ 85% deacetylation) were obtained from Sigma-Aldrich Chemical Co. Whatman chromatography paper no. 2 (58.0 cm × 68.0 cm) was obtained from GE Healthcare Worldwide (Pudong Shanghai, China) and used with further adjustment of size (A4 size). All chemicals and solvents were used as received with the analytical grade or above. Ultrapure water obtained from a Lichun water purification system ($\geqslant$18.25 MΩ cm, Jinan, China) was used in all assays and solutions.

2.2. Design of steric lab-on-chip device

The method for the fabrication of steric PMDs was adapted from our previous work [44,45]. The shape for wax-printing of this paper-based device was designed

using Adobe Illustrator CS4. As shown in Schemes 1, 2 and Fig. S2 (online), the 3D lab-on-paper device was composed of three electrodes, one screen-printed Ag/AgCl reference electrode (7 mm) (Scheme 1a(1)) and screen-printed carbon counter electrode (7 mm) (Scheme 1a(3)) on the reference tab (45 mm× 41 mm), one screen-printed carbon working electrode (5 mm) (Scheme 1b(6)) on working tab (45 mm× 41 mm). Two holes in reference tab (Scheme 1a(2)) were injection ports used to sample added. Another two holes in passageway tab were designed for reducing nonspecific adsorption of sample by the cellulose fibers. The crown-like paper-based hydrophobic regions in passageway tab (Scheme 1a(4)) were used as electrochemical cells to connect three-electrode system in one system. After being folded along the fold line, the steric lab-on-chip device was clamped between the circuit boards (Scheme 1d). Finally, the three electrodes will be connected once the paper electrochemical cell was filled with buffer solution. To better understand the flowing route of the sample, three dimensional stereogram of the paper-based device was drawn (Scheme 2). From the figure we can see, sample added into the hole of the reference tab flowed down to the hole in passageway tab, then reached working electrode. At the same time, the liquid in passageway tab flowed into the reference and counter electrodes through middle layer of the paper. Finally, three electrodes system was structured as expected.

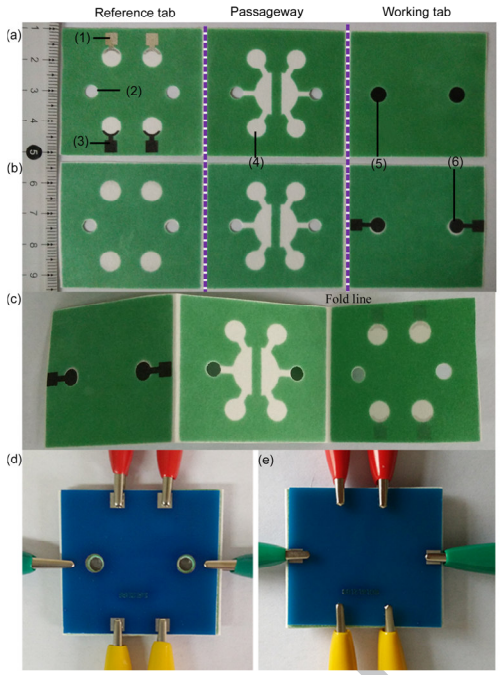

Scheme 1 (Color online) Design of the steric lab-on-chip device. Front (a) and back patterns (b) of this lab-on-chip device after baking, (1) screen-printed reference electrode, (2) via hole, (3) screen-printed carbon counter electrode, (4) crown-like paper-based hydrophobic regions, (5) rGO-PWE, (6) screen-printed carbon working electrode. (c) The steric lab-on-chip device was folded like the pictured here. (d) Photograph of the front and back (e) cover of constructed paper-based device clamped between the circuit boards.

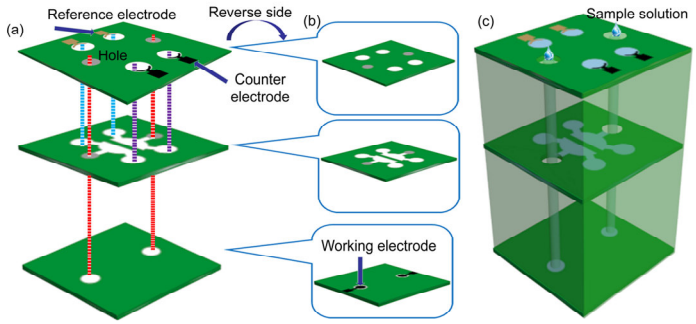

Scheme 2 (Color online) Fluid transmission route during this steric origami-based device. (a, b) The schematic representation mutual alignment of the three tabs after paper-based device was folded; (c) different concentrations of zinc ion were added into each injection ports in reference tab and the blue mark indicated invasion zone of the sample solution.

2.3. Synthesis of capture probe functionalized (Fe-P)$_n$-MOF

The (Fe-P)$_n$-MOF was prepared according to the previous literature with some revisions [46]. In a typical experiment, TCPP (39.54 mg), $FeCl_3 \cdot 6H_2O$ (40.55 mg), and HCl (0.1 mol/L) were added into a mixture containing a mixed solvent of DMF/ethanol (12 mL, 1:2 of v:v) with 40 min's ultrasonication. Next, the solution was heated in a Teflon-lined autoclave at 150 °C for 50 h. The browned crystals were collected by centrifugation and washed with DMF and ethanol for three times and then dried in vacuum at 60 °C. Then, 6.0 mg of (Fe-P)$_n$-MOF was dispersed in 1 mL of ethanol. The dispersion was added to a mixture containing 0.2 mL of ammonium hydroxide, 13.8 mL ethanol and 1.8 mL of tetramethoxysilane by stirring for 2 h at room temperature. Then the products were collected by centrifugation at 12000 rpm for 10 min and thoroughly washed by ethanol and dried under vacuum overnight. Subsequently, the obtained products were added into 4 mL of 20 mmol/L 3-mercaptopropyltrimethoxysilane (MPTS) ethanol solution and refluxed at 65 °C for 4 h. Finally, the product was collected by centrifugation and washed with water for four times and finally dried under vacuum at 50 °C for 12 h.

To further load Au NPs on MPTS modified (Fe-P)$_n$-MOF, 4 mL of Au NPs solution [47] was mixed with 1 mg of MPTS modified (Fe-P)$_n$-MOF with shaking for 3 h. The resulted composite was collected by centrifugation, and washed with water for several times.

A 90 μL of capture probe (10 μmol/L) solution activated with tris(2-carboxyethyl)-phosphine hydrochloride was added to the suspension of Au NPs-(Fe-P)$_n$-MOF and the mixture was stirred mechanically for 24 h. Afterwards, 6-mercapto-1-hexanol was used to block residual nonspecific active sites. Then, the product was dispersed in 0.5 mL of 50 mmol/L tris-acetate buffer (containing 0.3 mol/L NaCl, pH 7.0) and stored at 4 °C for use.

2.4. Preparation of rGO-PWE

Briefly, 0.5 mg/mL of GO nanosheets solution was sprayed onto the surface of the bare PWE and then dried in air. Then, the obtained paper was transferred to 0.1 mol/L Na_2SO_4 to electrochemically reduce GO at a constant potential of 0.9 V. After the electro-reduction reacted for 2,000 s, the rGO modified PWE was obtained and the resulted rGO-PWE electrodes were washed with ultrapure water.

2.5. Assay procedures on the steric lab-on-paper device

The detailed test procedures for the Zn^{2+} biosensor were represented in Fig. 1. First, 2.0 μL of 0.5 mg/mL chitosan was added into the rGO-PWE and naturally dried. Once activated with 2.0 μL of 2.5% glutaraldehyde for 30 min and washed with water, 10 μL of capture probe functionalized $(Fe\text{-}P)_n$-MOF (strand A) was applied to the paper working zone at 4 °C overnight. After blocking with 1% BSA for 40 min, 20 μL of substrate strands (strand C) were added to the capture-modified electrode and then incubated at 43 °C for 3 h. After rinsing with 50 mmol/L tris-acetate buffer (pH 7.0) to remove unbound oligonucleotides, 10 μL primer probe (strand B) was spread on the PWE and reacted at room temperature for 2 h, followed by washing twice with phosphate-buffered-saline (PBS) buffer. Then, 10 μL of reaction liquid, containing 1×ligase buffer, 0.2 U T4 ligase, and 50 nmol/L circular template probe, was deposited dropwise on the surface of the PWE and reacted for 1 h at 37 °C. The unbonded probe was rinsed out with doubly distilled water. Next, RCA reaction was initiated with the injection of 5 units of phi 29 DNA polymerase and dNTP (1.0 mmol/L) and continued for 1 h at 37 °C. Eventually, 0.4 mmol/L hemin was added and allowed to set undisturbed for 30 min and then the RCA reaction was finished (Fig. 1c1).

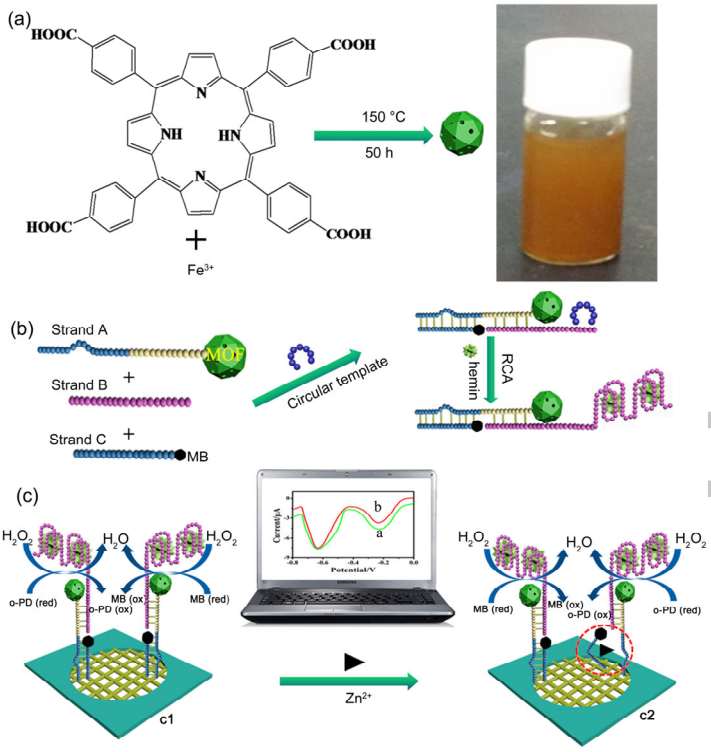

Fig. 1. (Color online) Illustration of the fabrication procedures for the (Fe-P)$_n$-MOF (a), RCA reaction (b) and detection mechanism (c).

Finally, 5.0 μL of $ZnCl_2$ solution with specified concentrations were added into the two surfaces of the working electrode at 37 °C for 40 min, followed by washing with PBS (Fig. 1c2). Then the paper was folded as Scheme 1c and clamped between the circuit boards (Scheme 1d) to fix and connect this paper based device to the electrochemical work station. At last, the electrochemical measurements were carried out in 5.0 μL of 0.1 mol/L PBS with 1.0 mmol/L H_2O_2 and 10 mmol/L o-PD. A differential pulse voltammetry scan from –0.8 to 0 V was performed to record the amperometric response for different concentrations of Zn^{2+}.

3. Results and discussion

3.1. Characterization of Au NPs-(Fe-P)$_n$-MOF and rGO-PWE

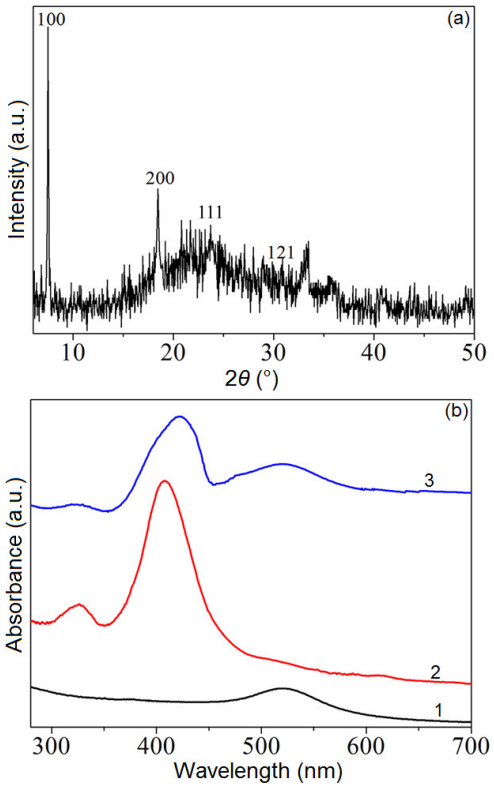

Fig. 2. (Color online) (a) XRD pattern of the (Fe-P)$_n$-MOF; (b) UV-vis absorption spectra of (1) Au NPs, (2) (Fe-P)$_n$-MOF, and (3) Au NPs-(Fe-P)$_n$-MOF.

The phase and structure of the synthesized products were examined by X-ray diffraction (XRD) (Fig. 2a). The diffraction peaks around 7.48°, 18.41°, 23.72° and 31.25° indexed to (100), (200), (111), and (121) planes, respectively, were observed [48], indicating the successful fabrication of (Fe-P)$_n$-MOF. Ultraviolet-visible (UV-vis) absorption spectra of Au NPs (curve 1 in Fig. 2b), (Fe-P)$_n$-MOF (curve 2 in Fig. 2b) and Au NPs-(Fe-P)$_n$-MOF (curve 3 in Fig. 2b) were plotted. The Au NPs revealed an obvious absorption peak at 520 nm. While, a visible Soret band at around 423 nm attributed to the coordination reaction between iron atoms and porphyrin was observed for (Fe-P)$_n$-MOF. As expected, two distinct adsorption peaks from Au NPs-(Fe-P)$_n$-MOF were observed in curve 3, suggesting the successful modification of Au NPs on (Fe-P)$_n$-MOF.

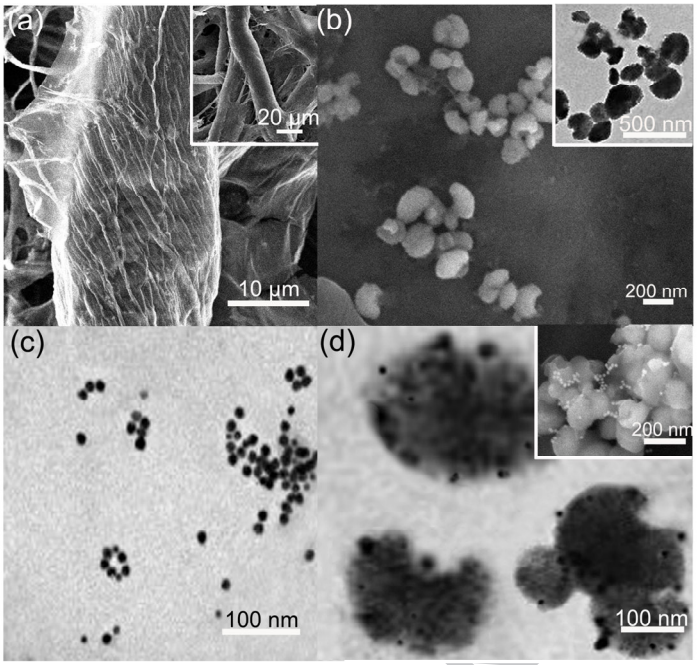

Fig. 3. SEM images of (a) rGO-PWE and (b) (Fe-P)$_n$-MOF; TEM images of Au NPs (c) and Au NPs-(Fe-P)$_n$-MOF (d). The inset of (a), (d), and (b) were SEM images of bare PWE, Au NPs-(Fe-P)$_n$-MOF, and TEM image of (Fe-P)$_n$-MOF, respectively.

The successful growth of rGO on cellulose fibers was confirmed by scanning electron microscopy (SEM) (Fig. 3a). An obviously continuous and dense rGO conducting layer on the cellulose fiber surface in paper sample zone was observed compared with the bare PWE (inset of Fig. 3a), indicated that rGO was successfully grown on the surfaces of the PWE. The morphology of the as-prepared (Fe-P)$_n$-MOF NPs was shown in Fig. 3b. It was distinctly found that crescent-like (Fe-P)$_n$-MOF NPs with the diameter of 180–300 nm were obtained from the SEM image. Inset of Fig. 3b presented the result of transmission electron microscopy (TEM) image of (Fe-P)$_n$-MOF, in which mono-disperse NPs could be easily identified. The Au NPs with an average diameter of 13 nm (Fig. 3c) were well dispersed on the surface of (Fe-P)$_n$-MOF matrix (Fig. 3d), indicating the successful modification of Au NPs on (Fe-P)$_n$-MOF using MPTS linker.

3.2. Feasibility of the ratiometric steric lab-on-paper device

A feasibility study of the steric lab-on-paper device at different electrodes in pH 7.0 nitrogen-saturated PBS containing 1.0 mmol/L H_2O_2 and 10 mmol/L o-PD was investigated (Fig. 4a). When the capture probe functionalized $(Fe\text{-}P)_n$-MOF was added into the working tab, a slight peak current at –0.64 V (curve 1) was observed，which came from the signal of o-PD in electrolyte. After the substrate probe was successively introduced on the proposed electrode, a new peak current at around -0.22 V appeared accordingly (curve 2), which was attributed to electroactive species MB linking to the surface of the PWE. However, noticeable increase in both of the electrochemical signal was observed after the RCA reaction (curve 3) because a good deal of H_2O_2 was catalyzed and turned into reactive oxygen species enhancing the current signal, which verified that the catalytic properties of MOF were raised substantially under the synergy catalysis of hemin/G-quadruplex. Additionally, in order to identify target responsive capability of the ratiometric steric lab-on-paper biosensor to Zn^{2+}, two concentrations of Zn^{2+} standard solution (100 and 300 nmol/L) were added into the electrolyte, respectively. The current signal at –0.22 V decreased gradually with increasing concentrations of Zn^{2+} (curves 4 and 5) because Zn^{2+} could be recognized by the capture probes, resulting in breakage of ribonucleic acid targets [49,50]. However, the current signal at -0.64 V was changed at the same time, which may be caused by the environmental interferences. To better understand the mechanism for the proposed biosensor, more detailed descriptions were shown in the supporting information.

Electrochemical impedance spectroscopy (EIS) could give the interface properties of the working electrodes in the assembly process, which was proceeded in a background solution of 0.1 mol/L PBS (pH 8.0) containing 5.0 mmol/L $[Fe(CN)_6]^{3-/4-}$ and 0.1 mol/L KCl. As shown in Fig.4b, after the rGO nanosheets and chitosan were grown onto PWE, the electron-transfer resistance (R_{et}) decreased significantly (curve 2) compared with bare PWE (curve 1), indicating that excellent conductivity was brought by rGO nanosheets and chitosan to promote the electron transfer. Noteworthy increase in the R_{et} value was observed with addition of capture probe (curve 3), 1% BSA (curve 4), substrate probe (curve 5) and primer probe (curve

6) on the surfaces of the chitosan modified rGO-PWE, suggesting the successful stepwise fabrication of the proposed biosensor. Further clearly increase of the R_{et} was observed after RCA reaction (curve 7), which might be caused by suppression of the formation of the numerous G-quadruplex structures, suggesting that this steric lab-on-paper biosensor was fabricated as expected.

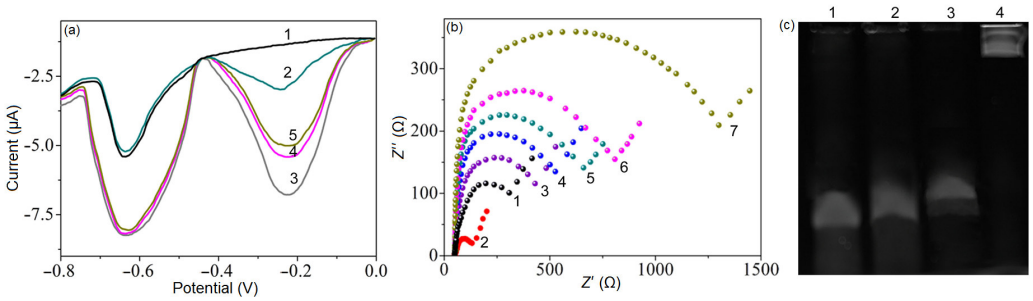

Fig. 4. (Color online) (a) Electrochemical responses of the stepwise fabrication of the lab-on-chip device; (b) Nyquist plots of the modified PWE at different stages; (c) Gel-electrophoresis analysis of the DNA. Hybridization of (lane 1) capture probe and substrate probe, (lane 2) capture probe, substrate probe and primer probe, (lane 3) capture probe, substrate probe, primer probe and circular template; lane 4: RCA products.

Besides, the gel electrophoresis experiments were utilized to further confirm the feasibility of the steric lab-on-paper device and the results were shown as Fig. 4c. When the capture probe and the substrate probe were mixed, a single strong spot (lane 1) was observed. After adding the primer probe to the above obtained sample, a band at a shorter electrophoresis distance was obtained (lane 2), which indicated that these three kinds of DNA probe hybridization reaction occured. After circular template probe was added, a new shorter electrophoresis distance was obtained (lane 3). Finally, the obtained RCA products showed extremely low mobility (lane 4) after RCA reaction reacted. Taken together, these tests demonstrated that our proposed method could be used for detection of Zn^{2+}.

Once again, the enhanced catalytic properties of MOF were proven by a macroscopic chromogenic reaction of 3,3´,5,5´-tetramethylbenzidine (TMB) using a

new paper-based device (Fig. S3 online). To ensure the accuracy of each measurement, the subjective steric configuration of paper used for colorimetric detection was identical with electrochemical detection. The differences were that three electrodes were not printed and one colorimetric detection zone was added for providing a place to carry out the chromogenic reaction. After the RCA reaction reacted, 10 μL of 20 mmol/L TMB and 3% H_2O_2 were added to the colorimetric zone. Then 20 μL of PBS was added into the electrochemical detection zone. The obtained results were shown in Fig. 5a. From the figure we can see, the intensity of chromogenic reaction was slight only when capture probe function alized $(Fe\text{-}P)_n$-MOF was present. Similarly, using capture probe-PWE as substrate, chromogenic strength was also insignificant after the RCA reaction. However, when the capture probe functionalized $(Fe\text{-}P)_n$-MOF and RCA products existed simultaneously, the substrate reaction was clear, which indicated that peroxidase-mimicking properties of the MOF were enhanced and the RCA process was conducted.

To further vertify RCA reaction indeed reacted on the PWE, carbon dots (Fig. S4 online) labelled DNA probe (the base sequence of this probe was shown in the supporting information) was employed to hybridize with the RCA products to produce a visual fluorescence signal. As described in Fig. 5b, a fairly high fluorescent signal was achieved with primer probe, circular template probe and carbon dots labelled DNA probe modified PWE, which not only indicated that the RCA reaction did react on the functional PWE but also proved that our developed method was feasible.

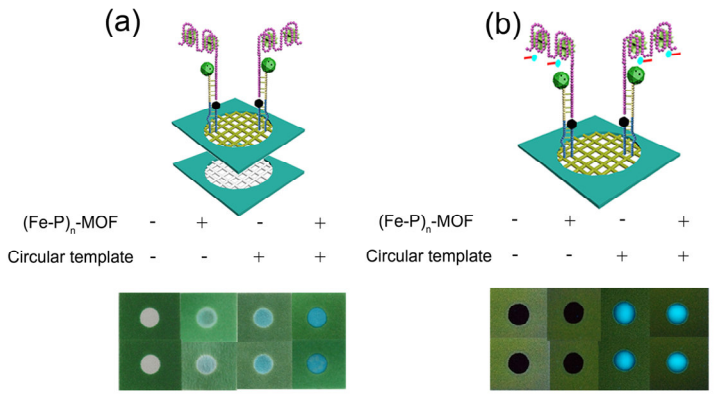

Fig. 5. (Color online) Performing RCA on the paper-based device. Detection of RCA products through: (a) colorimetric assay mediated by the RCA products; (b) photographs of carbon dots-labeled DNA oligonucleotide under fluorescent assay.

3.3. Electrochemical performance

The practical application properties of the steric lab-on-paper device were investigated. Under the optimal experimental conditions (Fig. S5 online), quantitative analysis of the Zn^{2+} concentration was based on the ratio of the current intensity of o-PD to the current intensity of MB intensity ($I_{-0.64}/I_{-0.22}$). When incubated with Zn^{2+}, the current at −0.22 V decreased with the increase of Zn^{2+} concentration, accompanied by changes in current intensities of the reference band at −0.64 V (Fig. 6a). We suspected that the intensity of current varies in -0.64 V may come from small environmental change of the working electrode placed. The linear relationship (Fig. 6b) could be represented as $I_{-0.64}/I_{-0.22} = 1.62\times10^{-4}\ c + 1.13$, with the correlation coefficient of R^2=0.997, where c was the value of Zn^{2+} concentration. The detection limit of the proposed ratiometric sensor was 0.03 nmol/L (S/N=3), with a linear range of 0.1−7,000 nmol/L, which was much lower than other sensors reported previously (Table 1). Compared with these methods, our developed sensor has a relatively large linear range and low detection limit.

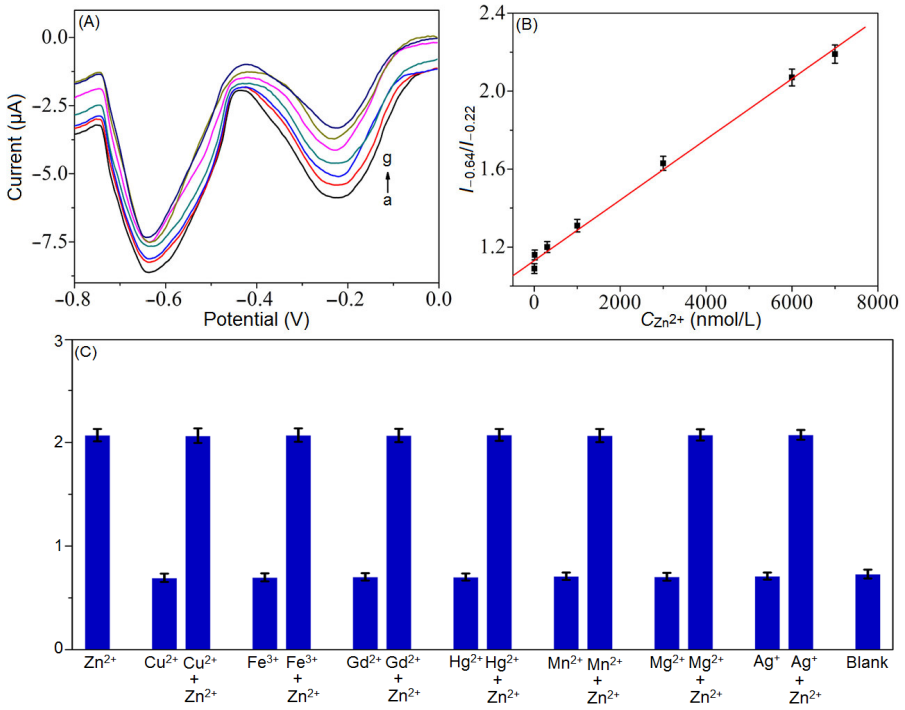

Fig. 6. (Color online) (A) Electrochemical responses of the system to different concentrations of Zn^{2+} (from a to g: 0.1, 10, 300, 1,000, 3,000, 6,000, 7,000 nmol/L) in N_2-saturated pH 7.0 PBS buffer containing 10 mmol/L o-PD, 1.0 mmol/L H_2O_2. (B) Linear plot of Zn^{2+} concentration versus the ratio of the current intensity of o-PD to MB. (C) Specificity of the biosensor over several metal ions. The biosensor was mixed with Zn^{2+} (6 μmol/L), other metal ions (0.6 mmol/L of Cu^{2+}, Fe^{3+}, Cd^{2+}, Hg^{2+}, Mn^{2+}, Mg^{2+}, Ag^{+}), blank solution and their corresponding mixture, respectively.

Table 1 Results of comparing with other immunoassay biosensing systems.

Detection methods	Linear range (nmol/L)	Detection limit (nmol/L)	Ref.
Stripping voltammetry	-	8	[51]
Fluorometric method	1−30	0.47	[14]
Fluorescent chemosensor	1,000−30,000	-	[52]
Electrochemical sensor	0.1−7,000	0.03	This study

The complexity of the environmental samples bring enormous challenges to the detection method for Zn^{2+} in sensitivity and selectivity. Therefore, to test the specificity and selectivity of our developed ratiometric steric lab-on-paper device, seven cations, including Cu^{2+}, Fe^{3+}, Cd^{2+}, Hg^{2+}, Mn^{2+}, Mg^{2+}, Ag^{+} and the mixture of Zn^{2+} and above seven cations, were examined and the obtained results were shown in Fig. 6c. The biosensor exhibited 3-fold higher current signal for Zn^{2+}, as compared to other metal ions with 100-fold higher concentration than Zn^{2+}. The excellent selectivity made the biosensor suitable for working in the complex biological system.

3.4. Zn^{2+} detection in cell extract

To verify the practical application of our developed steric lab-on-paper device, the device was applied to Zn^{2+} detection in HepG2 cells extract, which was prepared according to the previous literature [53]. The Zn^{2+} concentration in the samples was calculated to be 1.8±0.15 μmol/L by standard addition method. This value agreed well with that reported previously [14].

3.5. Zn^{2+} detection in real water samples

Table 2. The analysis of Zn^{2+} in real water samples (n=3)

Sample	Zn^{2+} added (nmol/L)	Zn^{2+} found (nmol/L)	Recovery (%)
1	1	0.91±0.12	91
2	5	5.08±0.17	102
3	10	10.13±0.19	101
4	15	15.26±0.14	102
5	20	21.07±0.05	105

The real-world applicability of the proposed platform is demonstrated once again by measuring five groups of water samples from our lab's tap. Then, recovery experiments of Zn^{2+} were conducted by spiking different concentrations of Zn^{2+} standard solution into 10-fold diluted real water samples. As shown in Table 2, the

recovery values were in the range of 91%–105%, indicating that our proposed biosensor could measure Zn^{2+} accurately in real samples.

4. Conclusion

In summary, a unique steric lab-on-paper device with hollow-channel was designed for simultaneous determination of dual analytes by intelligently designing the configuration of fluid flow passage. Interestingly, the environmental interferences could be eliminated ascribe to the built-in correction of ratiometric signal generated from o-PD existed in electrolyte, making the analytical result more accurate and reliable. It has been demonstrated that such devised paper-based device allows for the sensitively determination of zinc ion in HepG2 cells extract and real water sample with acceptable performance possessed. We believed that steric lab-on-paper device will serve as a powerful platform for basic scientific research, and will bring many convenience in a wide range of practical applications, such as, environmental monitoring, food safety and healthcare. Following the current work, further efforts will be made by us to improve the user-friendliness and suitability of on-site analysis applications, which will enable the practical use of steric lab-on-paper device by untrained end-users to easily achieve reliable analytical results.

Conflict of interest

The authors declare that they have no conflict of interest.

Acknowledgments

This work was supported by the National Natural Science Foundation of China (51502112, 21475052), Key Research and Development Program of Shandong Province, China (2016GGX102035), and Postdoctoral Science Foundation of University of Jinan, China (XBH1511).

References

[1] Rackus DG, Shamsi MH, Wheeler AR. Electrochemistry, biosensors and microfluidics: a convergence of fields. Chem Soc Rev 2015;44:5320-40.

[2] Chen L, Zhang CS, Xing D. Paper-based bipolar electrode-electrochemiluminescence (BPE-ECL) device with battery energy supply and smartphone read-out: a handheld ECL system for biochemical analysis at the point-of-care level. Sens Actuat B 2016;237:308-17.

[3] Fobel R, Kirby AE, Ng AHC, et al. Paper microfluidics goes digital. Adv Mater 2014;26:2838-43.

[4] Martinez AW, Phillips ST, Wiley BJ, et al. Flash: a rapid method for prototyping paper-based microfluidic devices. Lab Chip 2008;8:2146-50.

[5] Choi JR, Hu J, Tang RH, et al. An integrated paper-based sample-to-answer biosensor for nucleic acid testing at the point of care. Lab Chip 2016;16:611-21.

[6] Zhang Y, Ge SG, Liu HY, et al. Chemical and biochemical analysis on lab-on-a-chip devices fabricated using three-dimensional printing. Trends Anal Chem 2016; 85:166-80.

[7] Zhang Y, Li L, Zhang LN, et al. In-situ synthesized polypyrrole-cellulose conductive networks for potential-tunable foldable power paper. Nano Energy 2017;31:174-82.

[8] Renault C, Li X, Fosdick SE, et al. Hollow-channel paper analytical devices. Anal Chem 2013;85:7976-9.

[9] Renault C, Anderson MJ, Crooks RM. Electrochemistry in hollow-channel paper analytical devices, J Am Chem Soc 2014;136:4616-23.

[10] Li L, Zhang Y, Zhang LN, et al. Paper-based device for colorimetric and photoelectrochemical quantification of the flux of H_2O_2 releasing from MCF-7 cancer cells. Anal Chem 2016;88:5369-77.

[11] Li S, Wang YH, Ge SG, et al. Self-powered competitive immunosensor driven by biofuel cell based on hollow-channel paper analytical devices. Biosens Bioelectron 2015;17:18-24.

[12] Hu LH, Yang AP, Cui LM, et al. Fabrication of hyperbranched polyamine functionalized graphene for high-efficiency removal of Pb(II) and methylene blue. Chem Eng J 2016;287:545-56.

[13] Fang XF, Li JS, Li X, et al. Internal pore decoration with polydopamine nanoparticle on polymeric ultrafiltration membrane for enhanced heavy metal removal. Chem Eng J 2017;314:38-49.

[14] Li L, Fan YY, Tang B. Simultaneous imaging of Zn^{2+} and Cu^{2+} in living cells based on DNAzyme modified gold nanoparticle. Anal Chem 2015;87:4829-35.

[15] Duffner A, Weng L, Hoffland E, et al. Multi-surface modeling to predict free zinc ion concentrations in low-zinc soils. Environ Sci Technol 2014;48:5700-8.

[16] Woo H, You YM, Kim T, et al. Fluorescence ratiometric zinc sensors based on controlled energy transfer. J Mater Chem 2012;22:17100-12.

[17] Ning P, Jiang JC, Li LC, et al. A mitochondria-targeted ratiometric two-photon fluorescent probe for biological zinc ions detection. Biosens Bioelectron 2016;77:921-7.

[18] Yanaga M, Iwama M, Takiguchi K, et al. Determination of trace elements in organs and tissues of zinc deficient mice by instrumental neutron activation analysis. J Radioanal Nucl Chem 1998;231:187-9.

[19] Burdette SC, Walkup GK, Spingler B, et al. Fluorescent sensors for Zn^{2+} based on a fluorescein platform: synthesis, properties and intracellular distribution. J Am Chem Soc 2001;123:7831-41.

[20] Liu W, Cassano CL, Xu X, et al. Laminated paper-based analytical devices (LPAD) with origami-enabled chemiluminescence immunoassay for cotinine detection in mouse serum. Anal Chem 2013;85:10270-6.

[21] Liu H, Crooks RM. Paper-based electrochemical sensing platform with integral battery and electrochromic read-out. Anal Chem 2012;84:2528-32.

[22] Zhou HC, Long JR, Yaghi OM. Introduction to metal-organic frameworks. Chem Rev 2012;112:673-4.

[23] Mulfort KL, Hupp JT. Chemical reduction of metal-organic framework materials as a method to enhance gas uptake and binding. J Am Chem Soc 2007;129:9604-5.

[24] Huang XC, Lin YY, Zhang JP, et al. Ligand-directed strategy for zeolite-type metal-organic frameworks: zinc(II) imidazolates with unusual zeolitic topologies. Angew Chem Int Ed 2006;45:1557-9.

[25] Latroche M, Surblé S, Serre C, et al. Hydrogen storage in the giant-pore meta-organic frameworks MIL-100 and MIL-101. Angew Chem Int Ed 2006;45:8227-31.

[26] Seo JS, Whang D, Lee H, et al. A homochiral metal-organic porous material for enantioselective separation and catalysis. Nature 2000;404:982-6.

[27] Durette D, Bénard P, Zacharia R, Chahin R. Investigation of the hydrogen adsorbed density inside the pores of MOF-5 from path integral grand canonical Monte Carlo at supercritical and subcritical temperature. Sci Bull 2016; 61:594–600.

[28] Fu DL, Xu YY, Zhao M, et al. Enhancement of gas-framework interaction in a metal-organic framework by cavity modification. Sci Bull 2016; 61:1255–9.

[29] He XY, Gang MY, Li z, et al. Highly conductive and robust composite anion exchange membranes by incorporating quaternized MIL-101(Cr). Sci Bull 2017; 62:266–76.

[30] Chen B, Yang Y, Zapata F, et al. Luminescent open metal sites within a metal-organic framework for sensing small molecules. Adv Mater 2007;19:1693-6.

[31] Dong YQ, Cai JH, Fang QQ, et al. Dual-emission of lanthanide metal-organic frameworks encapsulating carbon-based dots for ratiometric detection of water in organic solvents. Anal Chem 2016;88:1748-52.

[32] Dinca M, Long JR. Hydrogen storage in microporous metal-organic frameworks with exposed metal sites angewandte. Angew Chem Int Ed 2008;47:6766-79.

[33] Lee J, Farha OK, Roberts J, et al. Metal-organic framework materials as catalysts. Chem Soc Rev 2008;38:1450-9.

[34] Ling PH, Lei JP, Zhang L, et al. Porphyrin-encapsulated metal-organic frameworks as mimetic catalysts for electrochemical DNA sensing via allosteric switch of hairpin DNA. Anal Chem 2015;87:3957-63.

[35] Hu ZC, Deibert BJ, Li J. Luminescent metal-organic frameworks for chemical sensing and explosive detection. Chem Soc Rev 2014;43:5815-40.

[36] O'Keeffe M, Yaghi OM. Deconstructing the crystal structures of metal-organic frameworks and related materials into their underlying nets. Chem Rev 2012;112:675-702.

[37] Wang XS, Chrzanowski M, Yuan DQ, et al. Covalent heme framework as a highly active heterogeneous biomimetic oxidation catalyst. Chem Mater 2014;26:1639-44.

[38] Perry JJ, Perman JA, Zaworotko MJ. Design and synthesis of metal-organic frameworks using metal-organic polyhedra as supermolecular building blocks. Chem Soc Rev 2009;38:1400-17.

[39] Zhang JW, Zhang HT, Du ZY, et al. Water-stable metal-organic frameworks with intrinsic peroxidase-like catalytic activity as a colorimetric biosensing platform. Chem Commun 2014;50:1092-4.

[40] Zhou L, Ou LJ, Chu X, et al. Aptamer-based rolling circle amplification: a platform for electrochemical detection of protein. Anal Chem 2007;79:7492-500.

[41] Zhang Z, Wang YY, Zhang NB, et al. Self-assembly of nucleic acid molecular aggregates catalyzed by a triple-helix probe for miRNA detection and single cell imaging. Chem Sci 2016;7:4184-9.

[42] Nie GM, Bai ZM, Yu WY, et al. Electrochemiluminescence biosensor based on conducting poly(5-formylindole) for sensitive detection of ramos cells. Biomacromolecules 2013;14:834-40.

[43] Huang HP, Tan YL, Shi JJ, et al. DNA aptasensor for the detection of ATP based on quantum dots electrochemiluminescence. Nanoscale 2010;2:606-12.

[44] Ge L, Wang SM, Yu JH, et al. Molecularly imprinted polymer grafted porous Au-paper electrode for an microfluidic electro-analytical origami device. Adv Funct Mater 2013;23:3115-23.

[45] Zhang Y, Ge L, Li M, et al. Flexible paper-based ZnO nanorod light-emitting diodes induced multiplexed photoelectrochemical immunoassay. Chem Commun 2014;50:1417-9.

[46] Jahan M, Bao Q, Loh KP. Electrocatalytically active graphene-porphyrin MOF composite for oxygen reduction reaction. J Am Chem Soc 2012;134:6707-13.

[47] Busbee BD, Obare SO, Murphy CJ. An improved synthesis of high-aspect-ratio gold nanorods. Adv Mater 2003;15:414-6.

[48] Cui L, Wu J, Li J, et al. Electrochemical sensor for lead cation sensitized with a DNA functionalized porphyrinic metal-organic framework. Anal Chem 2015;87:10635-41.

[49] Wang F, Elbaz J, Teller C et al. Amplified detection of DNA through an autocatalytic and catabolic DNAzyme-mediated process. Angew Chem Int Ed 2011;50:295-9.

[50] Zhang ZX, Balogh D, Wang F, et al. Smart mesoporous SiO_2 nanoparticles for the DNAzyme-induced multiplexed release of substrates. J Am Chem Soc 2013;135:1934-40.

[51] Malakhova NA, Stojko NY, Brainina KZ. Novel approach to bismuth modifying procedure for voltammetric thick film carbon containing electrodes. Electrochem Commun 2007;9:221-7.

[52] Xu ZC, Qian XH, Cui JN, et al. Exploiting the deprotonation mechanism for the design of ratiometric and colorimetric Zn^{2+} fluorescent chemosensor with a large red-shift in emission. Tetrahedron 2006;62:10117-22.

[53] Cheng Y, Huang Y, Lei JP, et al. Design and biosensing of Mg^{2+}-Dependent DNAzyme-Triggered ratiometric electrochemiluminescence. Anal Chem 2014;86:5158-63.